Deflection-Domain Passivity Control of Variable Stiffnesses Based On Potential Energy Reference

Michael Panzirsch[1], Marek Sierotowicz[1,2], Revanth Prakash[1], Harsimran Singh[1], Christian Ott[1]

***Abstract*—With emerging capabilities, robots will advance gradually into human environments in the near future. Thereby, safety and robustness is currently tackled through intrinsically soft robotics or variable impedances, mainly stiffnesses. In tele-operation, for instance, the control stiffness can be adapted to a measured arm impedance of the operator to stiffen the robot only when required for a manipulation task. Thus, humans or moving objects in the robot's environment are protected from hard collisions. Independent from its realization through hardware or software, the stability of the variation needs to be ensured through control strategies since energy is potentially introduced into the robotic system. This work presents a novel gradient-based passivity control concept for variable stiffnesses. In contrast to state-of-the-art methods, the approach is based on a potential energy storage reference and prevents phases of zero stiffness through deflection-domain control. I.e., according to the energy storage, the stiffness variation over the spring deflection is controlled to ensure passivity. Experiments confirm the functionality of the approach and its robustness against delayed communication and active environments.**

***Index Terms*—Safety in HRI, Variable Impedance, Telerobotics and Teleoperation, Deflection-Domain Control**

I. Introduction

SOFT robots with variable impedance joints [1], [2], [3] are one of the most promising concepts to guarantee safety in human-robot shared environments since – though being soft – they feature a high positioning accuracy and the ability to handle heavy loads. While moving without contacts, the robots can be controlled to be elastic in order to prevent humans and objects from unexpected harmful collisions. When grasping heavy objects or during other intended contacts with the environment, the robots can be controlled to be rigid for increased positioning accuracy.

Also in tele-operation, although a human is in the control loop, variable impedance (or tele-impedance [4]) increases the safety in active environments since the operator might not be aware of an impeding collision due to communication delay or weak visual perception. The desired coupling stiffness of the robot can then be varied according to the impedance of the operator's arm which can be observed, for instance, via surface electromyography (sEMG) [5], [4].

The evergreen challenge in variable impedance control is its non-passive behavior (which was already discussed in [6], [7]) in combination with its intrinsic time-varying characteristic. To ensure stability, this problem was tackled through different passivity control methodologies for a variety of applications.

In [5], the coupling stiffness was modulated through sEMG with an application in rehabilitation robotics. The concept was evaluated in an experimental tele-operation setup while the stability of the stiffness variation was only briefly discussed. Later, a comparable control setup was extended to tele-impedance including variable stiffness and damping observed from the human via sEMG [4]. Stability was guaranteed through the Time Domain Passivity Approach (TDPA) which was elaborated in more detail in [8]. Also, the energy-tank method [6], [9], [10] was applied to ensure mathematical passivity. In [6], a 6 degree-of-freedom (DoF) variable impedance control was proposed. The method of [9], considering a null space projection for tele-impedance in redundant manipulators was extended to contact tasks in [10].

One critical drawback of these state-of-the-art methods was already discussed in [7]. The control action of the TDPA and the energy tank methods can lead to a complete attenuation of the force command which corresponds to a zero coupling stiffness. This attenuation can persist over seconds depending on the delay or the system damping and motion respectively. In [7], a state-independent stability constraint which is applied to pre-planned impedance profiles is proposed as a solution. Thus, this concept is, for instance, not applicable to tele-operation scenarios in which the profile needs to be adaptive in real-time.

In this work, we propose a passive module for variable stiffness control which can be applied in combination with other passivity control principles as the wave-variable method [11], conventional TDPA [12] and modern TDPA [13] or energy tanks [6]. In contrast to the state-of-the-art, we propose the consideration of a potential energy storage which allows for a clear physical interpretation when compared to energy tanks. Furthermore, the approach ensures an arbitrary minimum stiffness while still being adaptive to stiffness profiles varying in real-time (in contrast to [7]). The concept is based on the observer-based gradient method (OBG) which was developed to adapt force feedback profiles depending on the deflection of the vitual spring of the coupling controller (deflection-domain control instead of time- or frequency-domain control) in case of delayed communication [14], [15], [16]. Here, this method

Manuscript received: September 09, 2021; Revised December 12, 2021; Accepted January 07, 2022.

This paper was recommended for publication by Editor Angelika Peer upon evaluation of the Associate Editor and Reviewers' comments.

The work was funded by the Bavarian Ministry of Economic Affairs, Regional Development and Energy, within the project SMiLE2gether(LABAY102).

[1]M. Panzirsch, M. Sierotowicz, R. Prakash, H. Singh and C. Ott are with the Institute of Robotics and Mechatronics in the German Aerospace Center (DLR), Wessling, Germany. michael.panzirsch@dlr.de

[2] M. Sierotowicz is also with the Chair of Medical Robotics, Department for Artificial Intelligence in Biomedical Engineering, Friedrich-Alexander University Erlangen-Nuremberg, 91052 Erlangen, Germany

Digital Object Identifier (DOI): see top of this page.

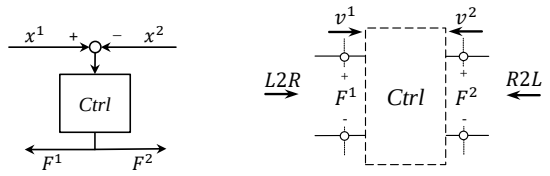

(a) Signal flow diagram. (b) Network representation.

Fig. 1: Coupling controller.

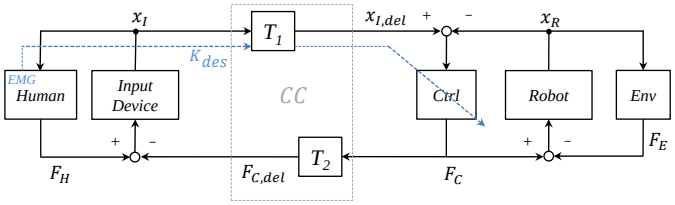

Fig. 2: Signal flow diagram for delayed tele-operation with variable stiffness.

is extended to stiffness profiles (OBG-K) and to guarantee passivity intrinsically.

The paper is structured as follows: Section II introduces the principles of tele-impedance and the drawbacks of the state-of-the-art. The concept and implementation of the proposed gradient-based method is presented in Section III. The experimental 1-DoF evaluation for tele-operation with delayed communication and active environments is presented in Section IV. Finally, Section V concludes the work.

II. Fundamentals and Problem Statement

Figure 1 presents the signal flow diagram and the network representation of a coupling controller *Ctrl*. In a tele-operation setup (compare signal flow diagram with variable impedance in Fig. 2), this controller couples the delayed *Input Device* pose $x_{I,del} = x^1$ with the *Robot* pose $x_R = x^2$. The poses x^1 and x^2 correspond to velocity v^1 and v^2 respectively. The controller force $F_C = F^1 = F^2$ is calculated via the controller stiffness and punishes a position deviation of *Input Device* and *Robot*. The controller force is therefore applied to the robot and sent as a feedback force to the *Input Device* side delayed by T_2. The desired stiffness K_{des} is measured by an EMG on the arm of the human operator and transmitted to the *Robot* side of the communication together with x_I and delayed by T_1.

At the port interfaces i of the 2-port network *Ctrl*, a power P^i can be calculated from the flows (velocities) v^i and the efforts (forces) F^i: $P^i(k) = F^i(k)v^i(k)$, in each time step k. With the sign of the power, the power flow in right-to-left ($R2L$) and left-to-right ($L2R$) direction can be determined:

$$P^i_{L2R}(k) = \begin{cases} 0, & \text{if } P^i(k) < 0, \\ P^i(k), & \text{if } P^i(k) > 0, \end{cases} \tag{1}$$

$$P^i_{R2L}(k) = \begin{cases} 0, & \text{if } P^i(k) > 0, \\ -P^i(k), & \text{if } P^i(k) < 0. \end{cases} \tag{2}$$

Via discrete time integration ($E^i(k) = \sum_{j=0}^{k} P^i(j)T_s$, with sampling time T_s), the respective energies E^i_{L2R} and E^i_{R2L} (positive by definition) can be found. The energy content E_{obs} of the *Ctrl* can be observed with:

$$\begin{aligned} E_{obs}(k) = E^1_{L2R}(k) + E^2_{R2L}(k) \\ - E^1_{R2L}(k) - E^2_{L2R}(k), \end{aligned} \tag{3}$$

where the input energies of the *Ctrl* are summed up and the output energies subtracted on the right side. Note that energy generation due to discretization is disregarded in this work assuming sufficiently high sampling rates.

With E_{obs}, the non-passive energetic behavior of the variable impedance can be observed. Fig. 3 describes this characteristic and the relation between observed and analytical energy $E_{an}(k) = 0.5K_{des}(k)\delta^2(k)$ with stiffness K and spring deflection δ. Hereon, δ represents the absolute value of the spring deflection $|\delta| = |x_{I,del} - x_R|$. For constant stiffness (see Fig. 3a), the observed energy equals the analytical energy over the full deflection range as visible from Fig. 3c. Fig. 3a and Fig. 3b present the variation of K over deflection δ since the proposed gradient method observes the energetic behavior of the variable impedance over time, but controls the energetic behavior over the deflection of the virtual spring (deflection-domain control). Here, δ_{max} denotes the arbitrary and time-varying deflection maximum during a deflection phase. When the stiffness increases constantly during a spring deflection δ (compare Fig. 3b), E_{an} remains non-negative, while E_{obs} becomes negative (see Fig. 3d), indicating a non-passive and potentially unstable behavior [7]. Note that E_{an} of Fig. 3d does not equal E_{an} of Fig. 3c due to the differing stiffness profiles.

This active behavior was tackled, for instance, through the energy-tank method and TDPA as discussed before. To ensure passivity in these approaches, the force output of the controller is attenuated which may lead to phases of zero effective stiffness. In case of unknown stiffness profiles, no state-of-the-art approach is able to ensure that no force attenuation (leading to zero stiffness phases) appears for arbitrary stiffness profiles. Exemplary, Fig. 5 depicts an experiment at zero delay with the energy-reflection based TDPA-ER [13] which is intrinsically able to passivate variable coupling stiffnesses. The network representation of the TDPA-ER is depicted in Fig. 6. The experiment was performed with the 1-DoF rotational devices introduced in Section IV and with deactivated OBG-K. The *Input Device* x_I moves the *Robot* x_R into two wall contacts (shaded areas).

The TDPA-ER calculates a reference energy storage E_{St} of the 2-port including communication channel *CC* and *Ctrl* from the input and output energies at port 3 and port 5. The E^{in}_{2port} and E^{out}_{2port} plots present the sum of these input and output energies and E_{2port} the overall energy sum. The reader is referred to [13] for more details. If the energy which exits at these ports exceeds E_{St}, the passivity controllers PCI and PCR dissipate this energy via a damping-based force attenuation such that the 2-port between port 2 and 6 is passive as marked in Fig. 6. It can be seen that when no energy is available in the reference energy storage E_{St} ($t = [47.3s, 47.8s]$ and $t = [52.2s, 53.1s]$), the force is completely attenuated to zero corresponding to a zero coupling stiffness which is visible from the high frequency disturbance

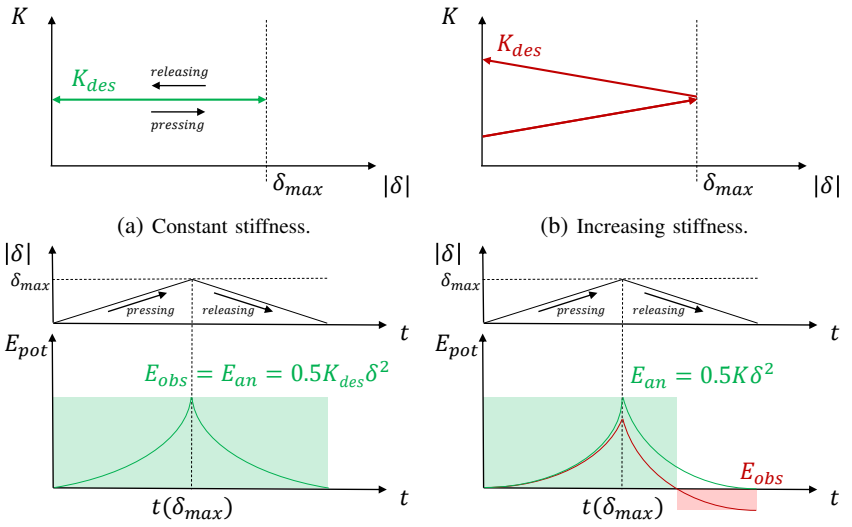

(a) Constant stiffness. (b) Increasing stiffness.

(c) Potential energies under constant stiffness. (d) Potential energies under increasing stiffness.

Fig. 3: Problem Statement: stiffness variation, spring deflection and resulting energetic behavior without passivity control.

(a) Passive stiffness limitation through K_{lim}

(b) Energies under passive stiffness limitation.

Fig. 4: Proposed solution: passive stiffness limitation and resulting energetic behavior with OBG-K.

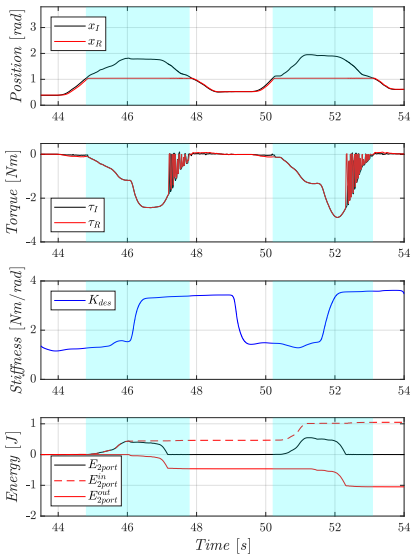

Fig. 5: Stiffness variation under TDPA-ER without OBG-K: passivity control through full force attenuation.

of the torque plots introduced by the passivity controller. Note that passive filters can reduce this disturbance but not prevent the full force attenuation and the resulting zero-stiffness phase. Due to the full force attenuation, the position convergence of x_I and x_R is reduced.

III. Proposed Approach

This section presents how an arbitrary real-time stiffness variation can be passivated in the deflection-domain with the proposed observer- and gradient-based control method OBG-K preventing zero-stiffness phases.

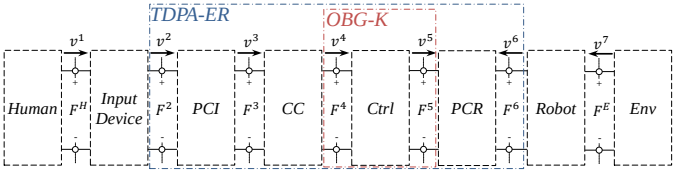

Fig. 6: Network representation for delayed tele-operation with TDPA-ER: The 2-port between port 2 and port 6 can be passivated by TDPA-ER. The Ctrl with variable stiffness can be designed to be intrinsically passive through OBG-K.

A. Concept Description

The control goal is to ensure that the *Ctrl* 2-port does not generate energy which is the case when the observed energy E_{obs} remains non-negative (compare Fig. 4b). To this end, the proposed method adapts the stiffness K_{des} to K_{lim} during one deflection phase with a variable deflection maximum δ_{max}. In a simplified first analysis, the spring stiffness is constantly increasing during the pressing phase ($\dot{\delta} > 0$) with gradient ∇K_{des}. Then, it is sufficient to decrease the stiffness to K_{lim} via the OBG-K during the releasing path according to the same gradient ∇K_{lim} as depicted in Fig. 4b. Thus, the resulting E_{obs}^{lim} does not become negative. In this case, the resulting energy curve E_{obs}^{lim} becomes symmetric w.r.t. δ_{max}.

However, Fig. 7 shows exemplary situations in which linear limiting functions K_{lim}^{lin} may lead to undesirably low (or even negative) K_{lim} values in contrast to polynomial limiting functions K_{lim}^{pol}. Here, we define an arbitrary value K_{zero} as the desired stiffness at the end of the deflection phase ($\delta_0 = 0$). Regarding K_{zero}, the linear solution is sufficient to guarantee $K_{lim}(\delta_0) \geq K_{zero}$ for the stiffness profile of Fig. 7a, while K_{lim}^{lin} cannot ensure that $K_{lim}(\delta_0) \geq K_{zero}$ in case of Fig. 7b. In such situations, polynomial functions can be applied to achieve $K_{lim}^{pol}(\delta_0) = K_{zero}$ as displayed in Fig. 7c.

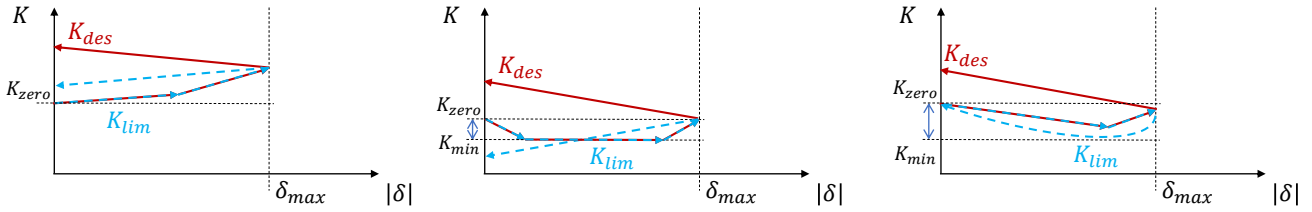

(a) Linear limiting function sufficient: $K_{lim}^{lin}(\delta_0) \geq K_{zero}$.

(b) Linear limiting function insufficient: $K_{lim}^{lin}(\delta_0) < K_{zero}$.

(c) Polynomial limiting function ensures: $K_{lim}^{pol}(\delta_0) = K_{zero}$.

Fig. 7: Limitations of linear limiting functions K_{lim}^{lin} and their elimination through polynomial limiting functions K_{lim}^{pol}.

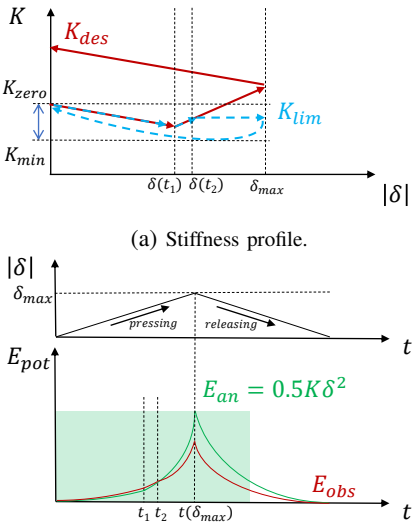

(a) Stiffness profile.

(b) Potential Energies.

Fig. 8: Passivity control with polynomial limiting function K_{lim}^{pol} with stiffness limitation during pressing path.

To avoid that the stiffness K_{lim}^{pol} drops too low ($K_{lim}^{pol}(\delta) < K_{min}$, with the desired minimum stiffness K_{min}) on the releasing path, the stiffness may need to be limited already on the pressing path as presented in Fig. 8a ($K_{lim}(\delta) \geq K_{min}$). Here, such a limitation on the pressing path ($t = [t_2, t(\delta_{max})]$) is implemented as $\nabla K_{lim} = 0$, but less conservative solutions are conceivable and should be evaluated in future work. Note that using linear limiting release functions K_{lim}^{lin} with such a limitation strategy during the pressing phase might lead to too conservative behavior.

Another more general remark is that inverting the stiffness profile of the pressing phase to apply it on the releasing phase is insufficient since several pressing and releasing actions can happen during one deflection phase.

The function for $K_{lim}(\delta)$ and the respective gradient $\nabla K_{lim}(\delta)$ on the releasing path have to be designed in each time step $k1$ according to the following conditions:

- Condition I: $K_{lim}(\delta_0) \geq K_{zero}$ at $\delta_0 = 0$ since the limitation curve should end higher than or at an arbitrary desired stiffness K_{zero},
- Condition II: $K_{lim}(\delta) \geq K_{min}$ to avoid too low stiffness values,
- Condition III: $E_{obs}(\delta_0) \geq 0$ at $\delta_0 = 0$,
- Condition IV: $K_{k1} = K_{act}(k1)$ since the limitation curve for the releasing path has to start at the current stiffness $K_{act}(k1)$.

Here, condition I, II and IV are related to the usability-optimized design of the searched limiting function while condition III ensures passivity. Note that the stiffness $K_{act}(k)$ which is finally set in the coupling spring is calculated as:

$$K_{act}(k) = min(K_{lim}(k), K_{des}(k)) \tag{4}$$

since the limited stiffness shall only be set if it is lower than the desired stiffness K_{des}.

Linear or arbitrary polynomial functions can be chosen for K_{lim}. Still, it can be assumed that in case of tele-operation, the function should be linear or the polynom's order should be as low as possible respectively to achieve a transparent behavior. In this work, we apply a constant gradient, as long as $K_{lim}^{lin}(\delta_0) \geq K_{zero}$ can be guaranteed and a polynomial function of the form $K_{lim}^{pol}(\delta) = a\delta^d + b\delta + c$ otherwise.

B. Linear K_{lim}^{lin} Function

In time step $k1$ of calculation, the linear equation of $K_{lim}^{lin}(\delta)$ with gradient ∇K_{lim}^{lin} is:

$$K_{lim}^{lin}(\delta) = \nabla K_{lim}^{lin}(\delta_{k1} - \delta) + K_{k1}, \tag{5}$$

with $\delta_{k1} = \delta(k1)$ and $K_{k1} = K_{act}(k1)$ of the current time step $k1$.

While the available energy $E_{obs}(k)$ has to be observed over time, the control happens with respect to the deflection δ (control in the deflection-domain).The variation of the potential energy $E_{lim}(\delta)$ over δ according to K_{lim}^{lin} can be found as:

$$\begin{aligned} E_{lim}(\delta_{k1}) &= \int_0^{\delta_{k1}} K_{lim}^{lin}(\xi)\xi d\xi \\ &= \frac{1}{6}\nabla K_{lim}^{lin}\delta_{k1}^3 + \frac{1}{2}K_{k1}\delta_{k1}^2. \end{aligned} \tag{6}$$

With $E_{lim}(\delta_{k1}) = E_{obs}(\delta_{k1})$, we can solve for the gradient ∇K_{lim}^{lin}:

$$\nabla K_{lim}^{lin} = \frac{6(E_{obs}(\delta_{k1}) - \frac{1}{2}K_{k1}\delta_{k1}^2)}{\delta_{k1}^3} \tag{7}$$

which ensures passivity. With $K_{lim}^{lin}(\delta_0) \geq K_{zero}$, it can be tested if the linear gradient suffices. At $\delta = 0$, K_{zero}, which will specify the aimed stiffness after a deflection phase, can be

freely chosen. Here, we set K_{zero} to the value of $K_{act}(\delta_0)$ at the beginning of the current spring deflection phase assuming that $K_{act}(\delta_0)$ also describes the desired minimum stiffness after the wall contact.

C. Polynomial K_{lim}^{pol} Function

If $K_{lim}^{lin}(\delta_0) \geq K_{zero}$ is not achieved, we apply a polynomial equation. Here, we propose $K_{lim}^{pol}(\delta)$ as:

$$K_{lim}^{pol}(\delta) = a\delta^d + b\delta + c. \tag{8}$$

One possibility to choose the exponent $d > 1$ is to search the lowest possible d that does not violate K_{min}. Alternatively, here, we choose $d = 2$ and limit K_{act} already on the pressing path in case the polynomial would violate K_{min} (assuming the releasing path started in the same time step, compare t_2 in Fig. 8a). The choice of the optimal limiting function depends largely on the application and the function complexity is mainly limited regarding computational efficiency.

The polynomial parameters a to c have to be determined according to the respective exponent d, K_{k1}, δ_{k1}, and $E_{obs}(\delta_{k1})$. With $K_{zero} = K_{act}(\delta_0)$, regarding (8), the parameter $c = K_{zero}$ is determined. $E_{lim}(\delta)$ is calculated as the integral of $K_{lim}^{pol}(\delta)\delta$ over the deflection range $[0, \delta]$:

$$\begin{aligned} E_{lim}(\delta) &= \int_0^{\delta} K_{lim}^{pol}(\xi)\xi d\xi \\ &= a\frac{1}{d+2}\delta^{d+2} + b\frac{1}{3}\delta^3 + c\frac{1}{2}\delta^2. \end{aligned} \tag{9}$$

With $E_{lim}(\delta_{k1}) = E_{obs}(\delta_{k1})$, solving (9) for b, we get:

$$b = \frac{E_{obs}(\delta_{k1}) - \frac{a}{d+2}\delta_{k1}^{d+2} - \frac{c}{2}\delta_{k1}^2}{\frac{1}{3}\delta_{k1}^3}. \tag{10}$$

Since $K_{lim}^{pol}(k1) = K_{act}(k1)$, fusing (8) and (10), we receive:

$$a = \frac{K_{k1} - c - \frac{3E_{obs}(\delta_{k1})}{\delta_{k1}^2} + \frac{3c}{2}}{\delta_{k1}^d(1 - \frac{3}{d+2})}. \tag{11}$$

Thus, with $c = K_{zero}$, $K_{lim}^{pol}(\delta)$ becomes

$$\begin{aligned} K_{lim}^{pol}(\delta) = &\frac{K_{k1} - K_{zero} - \frac{3E_{obs}(\delta_{k1})}{\delta_{k1}^2} + \frac{3K_{zero}}{2}}{\delta_{k1}^d(1 - \frac{3}{d+2})}\delta^d \\ &+ \frac{E_{obs}(\delta_{k1}) - \frac{a}{d+2}\delta_{k1}^{d+2} - \frac{K_{zero}}{2}\delta_{k1}^2}{\frac{1}{3}\delta_{k1}^3}\delta + K_{zero}. \end{aligned} \tag{12}$$

The respective gradient $\nabla K_{lim}^{pol}(\delta)$ can be calculated as:

$$\nabla K_{lim}^{pol}(\delta) = ad\delta^{d-1} + b. \tag{13}$$

Note that, due to (4), K_{act} can always be reduced by the user.

D. Implementation

This section describes the recommended implementation which was also applied in the subsequent experiments. Note that these recommendations might vary depending on the system specification, sampling time and encoder resolution.

- *Deflection Deadband:* Due to singularities in the equations, a minimum absolute spring deflection value $|\delta_{db}|$ should be chosen to ensure robustness. This value can be chosen low enough ensuring that no relevant energy generation (non-passive behavior) is missed. Within this deadband, $K_{act} = K_{des}$ holds and (here) the observed energy is reset to zero.
- *Pressing path:* To ensure performance sufficient for the respective application, exemplary, the minimum of K_{lim}^{pol} can be determined in each time step of the pressing path. In case this minimum goes below an arbitrary threshold K_{min}, the stiffness increase during the pressing can be completely canceled (A) or limited to a linear increase (B), for instance. Here, we choose option (A) to reduce complexity. A reasonable K_{min} can be determined from $K_{min} = K_{zero} - \Delta K_{JND}$, with the *just noticeable difference* in stiffness ΔK_{JND} [17].
- *Releasing path:*
  - Independent of the function type, the limiting stiffness function, e.g. (8), can be directly applied in the implementation during the releasing path instead of the gradient. The applied stiffness K_{act} is then chosen as the minimum of desired and limited stiffness: $K_{act} = min(K_{lim}, K_{des})$. This solution has shown to be more robust than the consideration of a gradient-based change of the current stiffness.
  - If a constant gradient or linear limiting function suffices ($K_{lim}^{lin}(\delta = 0) \geq K_{zero}$), it should be preferred to a polynomial function $K_{lim}^{pol}(\delta)$ since it promises to display a more transparent behavior to the user. This may also lead to an increasing K_{lim} on the releasing path which is admissible since $K_{act} = min(K_{lim}, K_{des})$.
  - Otherwise, the limiting polynomial function (8) should be chosen to prevent undesired small stiffness minima.
- *Filter:* The detection of a releasing and pressing phase can be filtered for increased robustness. Here, we account a change between the phases if the change was of a minimum amplitude in $\Delta_{min}\delta$ and was maintained for a minimum time t_{min}.
- *Desired stiffness estimation:* The desired stiffness is estimated using a Random Fourier Feature regression algorithm [18]. The prediction is filtered through an adaptive lowpass filter, which calculates its cutoff frequency based on the current magnitude of the signal and the magnitude of its first time derivative. The purpose of the filter is to stabilize the estimated desired stiffness K_{des}, which is otherwise prone to degradation during prolonged muscle contractions due to noise properties of the EMG measurement, such as heteroskedasticity [19]. The filter is especially tuned to ensure stability in the experiment described in Section IV, which involves several prolonged muscle contractions.
- *Coupling Controller Damping:* In the presented experiments, we set the virtual coupling controller damping B to zero and apply a virtual spring only in order to present the most conservative control solution. Still, with the presented 2-port equations for energy observation, a

Fig. 9: Myo Armband from *Thalmic Labs*: an 8-channel EMG sensor used to predict the desired wrist stiffness K_{des}.

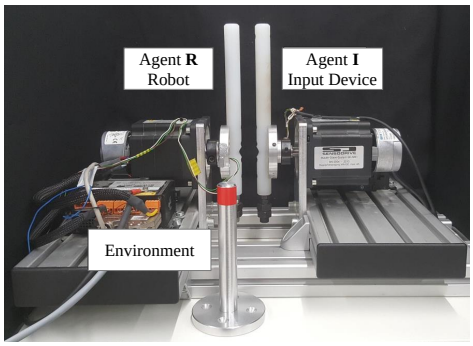

Fig. 10: Experimental setup: two 1-DoF rotational devices.

virtual damping can be directly added along with the virtual spring. Case 1: When energy dissipated by the damping is considered in $E_{obs}(k)$, the energies should be reset at zero deflection as discussed before to avoid energy accumulation. Case 2: Alternatively, a coupling controller damping can be used while only the potential energy is stored in E_{obs}. This would not affect the functionality of the OBG-K and not violate passivity.

IV. Experimental Evaluation

The following experiments were performed with the 1-DoF devices depicted in Fig. 10. The control principle was implemented in Matlab/Simulink and running on a QNX system at 1kHz sampling rate. The EMG from the user's forearm is sampled on 8 channels at a 200 Hz rate using a Myo Armband by *Thalmic Labs*, shown in Fig. 9. The desired stiffness is estimated through a Random Fourier Features (RFF) kernel applied to a ridge regression [18]. The estimated desired stiffness of the wrist K_{des} is outputted at the a 200Hz rate. The RFF algorithm, together with a gain and offset parameters, ensures that the condition $1.2Nm/rad < K_{des} < 4.5Nm/rad$ is maintained at all times. As mentioned before, though possible, no virtual coupling controller damping, but only local damping is applied.

The first set of experiments (see Fig. 11a-11c) consists in an analysis of the OBG-K performance for different K profiles. The subsequent experiment of Fig. 12 presents the robustness against active environments and Fig. 13 the performance of OBG-K with TDPA-ER at variable delay.

The plots of Fig. 11 show free motions of *Input Device* x_I and *Robot* x_R as well as wall contacts of the *Robot*. The plots of Fig. 11a present a tele-operation scenario in which the desired stiffness is decreased during the contact (compare light shaded area). The energy plot shows that the observed potential energy E_{obs} is higher than the analytical energy E_{an} indicating a dissipating effect of the stiffness profile. Therefore, no limitation of K_{des} is required. Note that E_{obs} is set to zero in the $|\delta_{db}|$-range at $t \approx 41.75s$ such that the potential energy is zero when the spring is not loaded. This is mathematically not necessary to ensure passivity but leads to a physically reasonable behavior in contrast to other state-of-the-art approaches. τ_{des} is the torque which would result from K_{des}. The energies E^{in}_{2port} and E^{out}_{2port} describe the input and output energies of the coupling controller 2-port.

The experiment of Fig. 11b presents a complex stiffness variation during contact. At $t \approx [57.9, 58.05]$, a stiffness increase is prevented (constant K_{act}) since the approach detected that a violation of K_{min} might appear. During the release phase, K_{act} is limited by the OBG-K which exactly ensures passivity (compare plot of E_{obs}). Also, analogous to the described design, K_{act} reaches K_{zero} at $\delta \approx 0$. When $|\delta_{db}|$ is reached, K_{act} is reset to K_{des}. Due to the low spring deflection at that instant, neither a critical energy injection nor a perceivable torque jump (see plot of τ) results from this reset.

Figure 11c presents a small stiffness variation during the contact outlining the robustness of the approach against potentially noisy position or stiffness signals. The functionality is analogous to Fig. 11b and passivity is confirmed by E_{obs}.

In experiment Fig. 12, first the operator moves the *Robot* against a wall ($t = [33.5s, 35.2s]$) under increasing stiffness. Afterwards, an active environment (second operator hand) moves the *Robot* which controls the *Input Device* (dark shaded area) in free motion and into a wall contact at $t = [37s, 40.5s]$. The *Input Device* is released during this procedure. It can be observed that the energy E_{2port} is non-negative confirming that the deadband of $|\delta_{db}|$ is not critical in terms of passivity. Due to the energy input from the active environment, the input and output energies E^{in}_R, E^{out}_R, E^{in}_I, and E^{out}_I from robot and input device are presented separately. Since the released *Input Device* has less local damping than the *Robot*, small oscillations can be observed in the position and torque plots before and after the wall contact of the *Input Device*. These oscillations vanish when the *Input Device* is grasped or the same virtual local damping is implemented as on the *Robot* side. The experiment confirms that the OBG-K operates correctly in case of active environments. The high performance of the control method under such critical circumstances promises a high robustness and applicability to a large variety of robotic scenarios. The energy plots $E^{w/oOBG-K}_{2port}$ in Fig. 12 and 13 present the energy behavior of the coupling spring which would result if K_{des} was set instead of K_{lim}. In the phases where this energy is negative (compare darker shaded areas), the TDPA-ER without OBG-K would attenuate the forces completely resulting in zero-stiffness phases.

Finally, the experiment of Fig. 13 was performed with the OBG-K in combination with TDPA-ER to ensure passivity despite delayed communication (50ms round-trip delay). During the first wall contact (light shaded areas), K_{des} was reduced, during the second, K_{des} was kept constant and increased during the third contact. The dark shaded area presents the behavior in case of active environments. It can be observed that the passivity of the variable stiffness 2-port is maintained

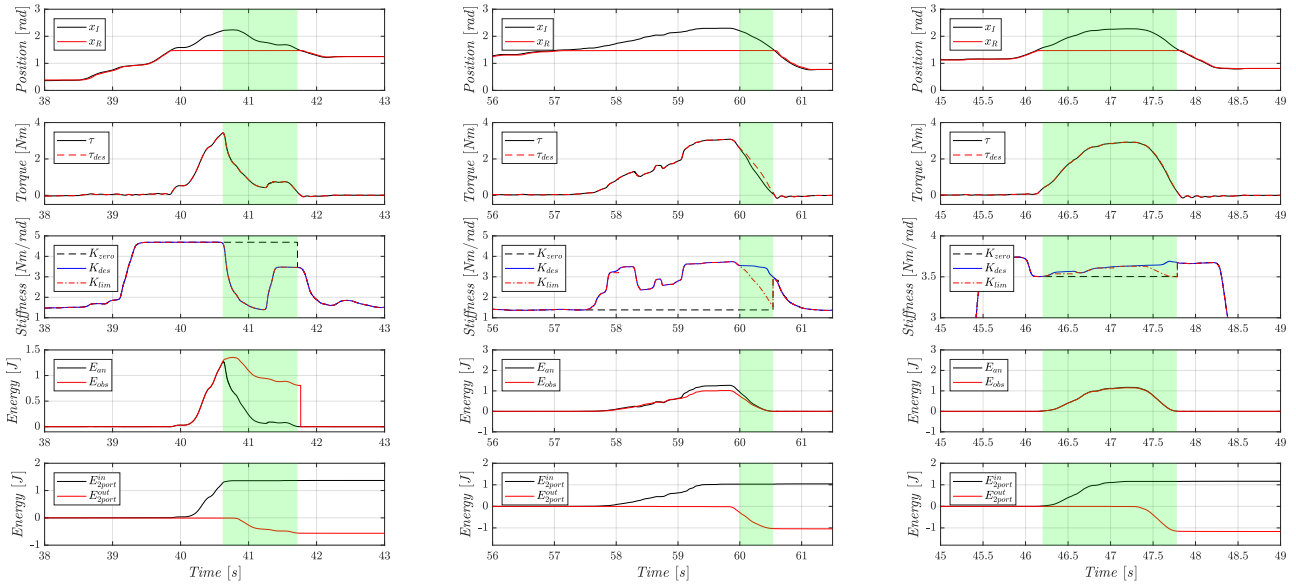

(a) Results for OBG-K in case of K_{des} decrease during pressing phase.

(b) Results for OBG-K in case of K_{des} increase during pressing phase.

(c) Results for OBG-K in case of small K_{des} variation during contact.

Fig. 11: Results for OBG-K in case of different stiffness variation profiles with passive environment.

(compare $E_{2port} \geq 0$). Still, the torque feedback to the operator is attenuated to zero by the TDPA-ER (due to energy generation by the communication delay at $t = [17s, 17.2s]$) leading to a reduced stiffness impression for the operator. This short disturbance can be reduced by a passive filter which was not applied here for ease of interpretation. A combination of OBG-K with [20] promises to circumvent this effect of force attenuation and should be investigated in future work. Note that $E_{2port}^{w/oOBG-K}$ refers to the OBG-K 2-port whereas E_{2port} refers to the TDPA-ER 2-port of Fig. 6.

Discussion

Analyzing the behavior of the approach from a tele-operation perspective, it can be argued that the control functionality of the presented approach does not lead to a critically reduced usability. It can be assumed that in tele-operation scenarios, an operator generally increases the stiffness of the arm while preparing for and pushing against a contact, while the operator arm softens when the operator wants to move the robot out of the contact. Thereby, the spring load helps the operator and the operator intentionally reduces the arm stiffness to be lead by the spring.

Especially in case of fast stiffness increases (with respect to exponent d), the chosen limitation during the pressing phase may be too conservative. Limiting the increase curve depending on the chosen exponent d seems to be a promising solution to reduce this conservatism and should be investigated in future work. At the same time, the reliable stable behavior resulting from the physically conceivable control principle ensures the OBG-K applicability to a large set of scenarios.

Here, the energy generation inside the deflection deadband was analyzed as negligibly low and its robustness regarding communication delay and active environments could be confirmed. Still, in future work, the applicability to hardware with other dynamic properties needs to be investigated.

V. Conclusion and Future Work

This work presents the first control concept ensuring passivity and non-zero stiffness for unknown stiffness variation profiles. In contrast to earlier methods, the approach is based on potential energy observation presenting a physically well comprehensible concept. While variable stiffness profiles could only be handled through force attenuation leading to perceivable phases of zero stiffness in state-of-the-art approaches, the proposed approach is able to ensure a selected minimum stiffness independent of the interaction and stiffness profile. Also, in contrast to methods as, for instance, those based on energy-tanks, no initial energy storage is required for sufficient performance.

The 1-DoF experiments confirmed the passivity of the approach and its robustness against delay and active environments. The next development steps should include the developments of new concepts for limitation during the pressing phase, the extension to 6-DoF setups and the application in realistic scenarios.

Acknowledgment

The work was funded by the Bavarian Ministry of Economic Affairs, Regional Development and Energy, within the project SMiLE2gether(LABAY102).

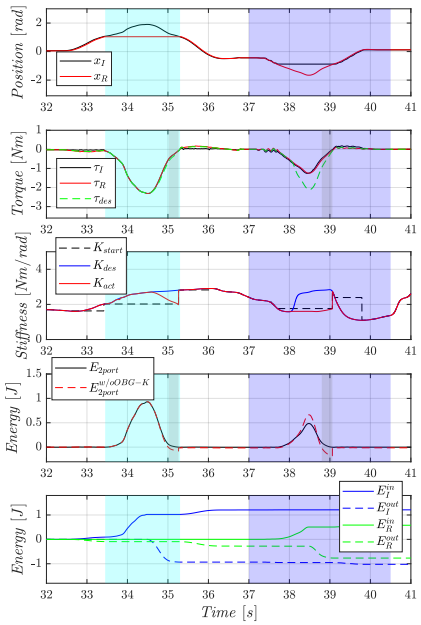

Fig. 12: Results for OBG-K in case of K_{des} increase during pressing phase with active environment.

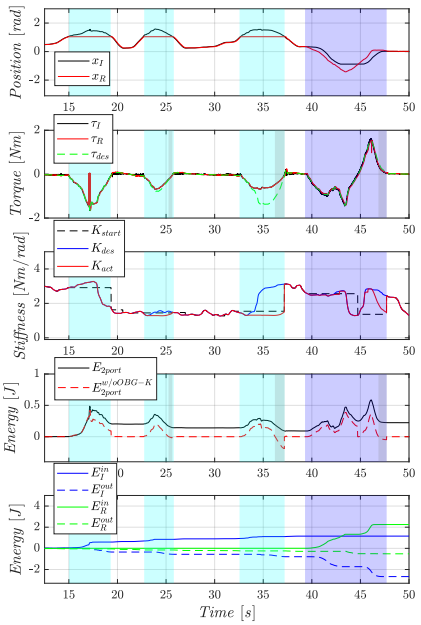

Fig. 13: Results for combination of OBG-K and TDPA-ER at 50ms roundtrip-delay: different K_{des} variation profiles and active environment.

REFERENCES

[1] T. Morita, H. Iwata, and S. Sugano, "Development of human symbiotic robot: Wendy," in *Proceedings 1999 IEEE International Conference on Robotics and Automation (Cat. No. 99CH36288C)*, vol. 4. IEEE, 1999, pp. 3183–3188.

[2] J. W. Hurst, J. E. Chestnutt, and A. A. Rizzi, "An actuator with physically variable stiffness for highly dynamic legged locomotion," in *IEEE International Conference on Robotics and Automation, 2004. Proceedings. ICRA'04. 2004*, vol. 5. IEEE, 2004, pp. 4662–4667.

[3] S. Wolf, O. Eiberger, and G. Hirzinger, "The dlr fsj: Energy based design of a variable stiffness joint," in *2011 IEEE International Conference on Robotics and Automation*. IEEE, 2011, pp. 5082–5089.

[4] M. Laghi, A. Ajoudani, M. Catalano, and A. Bicchi, "Tele-impedance with force feedback under communication time delay," in *2017 IEEE/RSJ International Conference on Intelligent Robots and Systems (IROS)*. IEEE, 2017, pp. 2564–2571.

[5] C. Castellini, A. Arquer, and J. Artigas, "semg-based estimation of human stiffness: Towards impedance-controlled rehabilitation," in *5th IEEE RAS/EMBS International Conference on Biomedical Robotics and Biomechatronics*. IEEE, 2014, pp. 604–609.

[6] F. Ferraguti, C. Secchi, and C. Fantuzzi, "A tank-based approach to impedance control with variable stiffness," in *2013 IEEE International Conference on Robotics and Automation*. IEEE, 2013, pp. 4948–4953.

[7] K. Kronander and A. Billard, "Stability considerations for variable impedance control," *IEEE Transactions on Robotics*, vol. 32, no. 5, pp. 1298–1305, 2016.

[8] M. Laghi, A. Ajoudani, M. G. Catalano, and A. Bicchi, "Unifying bilateral teleoperation and tele-impedance for enhanced user experience," *The International Journal of Robotics Research*, vol. 39, no. 4, pp. 514–539, 2020.

[9] Y. Michel, C. Ott, and D. Lee, "Passivity-based variable impedance control for redundant manipulators," in *in Proc. IFAC World Congress (IFAC)*, 2020.

[10] Y. Michel, R. Rahal, C. Pacchierotti, P. R. Giordano, and D. Lee, "Bilateral teleoperation with adaptive impedance control for contact tasks," *IEEE Robotics and Automation Letters*, vol. 6, no. 3, pp. 5429–5436, 2021.

[11] G. Niemeyer and J.-J. Slotine, "Stable adaptive teleoperation," *IEEE Journal of oceanic engineering*, vol. 16, no. 1, pp. 152–162, 1991.

[12] J.-H. Ryu and C. Preusche, "Stable bilateral control of teleoperators under time-varying communication delay: time domain passivity approach," in *Proc. of 2007 IEEE International Conference on International Conference on Robotics and Automation*. IEEE, 2007, pp. 3508–3513.

[13] M. Panzirsch, J.-H. Ryu, and M. Ferre, "Reducing the conservatism of the time domain passivity approach through consideration of energy reflection in delayed coupled network systems," *Mechatronics*, vol. 58, pp. 58–69, 2019.

[14] H. Singh, A. Jafari, and J.-H. Ryu, "Enhancing the force transparency of time domain passivity approach: Observer-based gradient controller," in *2019 International Conference on Robotics and Automation (ICRA)*. IEEE, 2019, pp. 1583–1589.

[15] H. Singh, M. Panzirsch, and J.-H. Ryu, "Preserving the physical coupling in teleoperation despite time delay through observer-based gradient control," *IFAC-PapersOnLine*, vol. 52, no. 18, pp. 25–30, 2019.

[16] M. Panzirsch, H. Singh, and C. Ott, "The 6-dof implementation of the energy-reflection based time domain passivity approach with preservation of physical coupling behavior," *IEEE Robotics and Automation Letters*, vol. 5, no. 4, pp. 6756–6763, 2020.

[17] A. Schiele, M. Aiple, T. Krueger, F. van der Hulst, S. Kimmer, J. Smisek, and E. den Exter, "Haptics-1: Preliminary results from the first stiffness jnd identification experiment in space," in *International Conference on Human Haptic Sensing and Touch Enabled Computer Applications*. Springer, 2016, pp. 13–22.

[18] A. Gijsberts, R. Bohra, D. Sierra González, A. Werner, M. Nowak, B. Caputo, M. A. Roa, and C. Castellini, "Stable myoelectric control of a hand prosthesis using non-linear incremental learning," *Frontiers in neurorobotics*, vol. 8, p. 8, 2014.

[19] G. Rasool, N. Bouaynaya, and K. Iqbal, "Muscle activity detection from myoelectric signals based on the ar-garch model," in *2012 IEEE Statistical Signal Processing Workshop (SSP)*. IEEE, 2012, pp. 420–423.

[20] H. Singh, M. Panzirsch, A. Coelho, and C. Ott, "Proxy-based approach for position synchronization of delayed robot coupling without sacrificing performance," *IEEE Robotics and Automation Letters*, vol. 5, no. 4, pp. 6599–6606, 2020.